Published in final edited form as:
J Bone Miner Res. 2014 March ; 29(3): 693–704. doi:10.1002/jbmr.2079.

Increased osteopontin contributes to inhibition of bone mineralization in FGF23-deficient mice

Quan Yuan, DDS PhD[1,2], **Yan Jiang, MD**[1,3], **Xuefeng Zhao, DDS**[1,2], **Tadatoshi Sato, PhD**[1], **Michael Densmore, MS**[1], **Christiane Schüler**[4], **Reinhold G. Erben, MD VMD**[4], **Marc D. McKee, PhD**[5], and **Beate Lanske, PhD**[1,*]

[1]Department of Oral Medicine, Infection & Immunity, Harvard School of Dental Medicine, Boston, MA, 02115

[2]State Key Laboratory of Oral Diseases, West China Hospital of Stomatology, Sichuan University, Chengdu, PR China

[3]Department of Endocrinology, Peking Union Medical College Hospital, Beijing, PR China

[4]Department of Biomedical Sciences, University of Veterinary Medicine, Vienna 1210, Austria

[5]Faculty of Dentistry, and Department of Anatomy & Cell Biology, McGill University, Montreal, Quebec, Canada

Abstract

Excessive FGF23 has been identified as a pivotal phosphaturic factor leading to renal phosphate-wasting, and the subsequent development of rickets and osteomalacia. In contrast, loss of FGF23 in mice (*Fgf23*$^{-/-}$) leads to high serum phosphate, calcium and 1,25-vitamin-D levels resulting in early lethality attributable to severe ectopic soft-tissue calcifications and organ-failure. Paradoxically, *Fgf23*$^{-/-}$ mice exhibit a severe defect in skeletal mineralization despite high levels of systemic mineral ions and abundant ectopic mineralization, an abnormality that remains largely unexplained. Through use of *in situ* hybridization, immunohistochemistry and immunogold labeling coupled with electron microscopy of bone samples we discovered that expression and accumulation of osteopontin (*Opn*/OPN) was markedly increased in *Fgf23*$^{-/-}$ mice. These results were confirmed by qPCR-analyses of *Fgf23*$^{-/-}$ bones and ELISA measurements of serum OPN. To investigate whether elevated OPN levels were contributing to the bone mineralization defect in *Fgf23*$^{-/-}$ mice, we generated *Fgf23*$^{-/-}$/*Opn*$^{-/-}$ double-knockout mice (*DKO*). Biochemical analyses showed that the hypercalcemia and hyperphosphatemia observed in *Fgf23*$^{-/-}$ mice remained unchanged in *DKO* mice, however μCT and histomorphometric analyses showed a significant improvement in total mineralized bone-volume. The severe osteoidosis was markedly reduced and a normal mineral apposition rate was present in *DKO* mice, indicating that increased OPN levels in *Fgf23*$^{-/-}$ mice are at least in part responsible for the osteomalacia. Moreover, the increased OPN levels were significantly decreased upon lowering serum phosphate by feeding low phosphate diet or deletion *NaPi2a*, indicating phosphate attributes in part to the high OPN levels in *Fgf23*$^{-/-}$ mice. In summary, our results suggest that increased OPN is an important pathogenic factor mediating the mineralization defect and the alterations in bone metabolism observed in *Fgf23*$^{-/-}$ bones.

[*]Corresponding author: Beate Lanske, Department of Oral Medicine, Infection and Immunity, Harvard School of Dental Medicine, Research and Education Building, Room 303, 188 Longwood Avenue, Boston, MA 02115, phone: (617) 432 5748, fax: (617) 432 5767, beate_lanske@hsdm.harvard.edu.

Authors' roles: Study design: QY and BL. Study conduct: QY, YJ, XZ, MD and MDM. Data collection: QY, YJ, XZ, MD, MDM and CS. Data analysis: QY, BL, RGE, and MDM. Data interpretation: QY, BL, RGE, and MDM. Drafting manuscript: QY, BL, and MDM. Revising manuscript content: BL and MDM. Approving final version of manuscript: BL and MDM. BL, MDM, and RGE take responsibility for the integrity of the data analysis.

Introduction

FGF23, a member of the FGF19 subfamily of fibroblast growth factors, has been shown to play a key role in balancing mineral ion homeostasis (1–4). Consequently, it has been implicated in the pathogenesis of various phosphate-wasting diseases, including autosomal dominant hypophosphatemic rickets (ADHR) (5), X-linked hypophosphatemia (XLH) (6), oncogenic osteomalacia (OOM) (7), chronic kidney disease (CKD) (8), familial tumoral calcinosis (FTC) (9), McCune-Albright syndrome and fibrous dysplasia of bone (10, 11).

FGF23 is mainly secreted by bone cells (11–13) and its function is dependent on an interaction with the co-factor Klotho (14–16). Together, these form a complex with FGF receptor 1c (FGFR1c), thereby converting this otherwise canonical FGF receptor into a receptor specific for FGF23 (15). FGF23 uses the FGFR1c/Klotho complex to directly target the kidney where it induces phosphate wasting by decreasing the expression of the sodium-dependent phosphate co-transporters NaPi2a and NaPi2c (17, 18).

Recent studies (18, 19) have demonstrated that overexpression of FGF23 in mice leads to hyposphosphatemia and hyperphosphaturia. Conversely, mice lacking FGF23 function (*Fgf23*$^{-/-}$) exhibit a phenotype that includes profound growth retardation, muscle wasting, infertility, atherosclerosis, extensive soft tissue calcifications, pulmonary emphysema, general tissue atrophy, severely shortened lifespan, and biochemical disorders including hyperphosphatemia, hypercalcemia, high serum 1,25$(OH)_2$D levels, and decreased serum PTH levels (20–22). Despite the presence of such a high serum mineral ion content and even the presence of severe soft tissue calcifications (23, 24), *Fgf23*$^{-/-}$ mice present with severe defects in skeletal mineralization (osteomalacia/osteoidosis). The reason for this reduced skeletal mineralization occurring in the presence of high serum calcium and phosphate is largely unknown, but such observations suggest an accumulation of a mineralization inhibitor locally within the extracellular matrix of bone.

FGF23 itself has been demonstrated to be an inhibitor of mineralization, but whether it acts directly or indirectly is not yet known. Wang *et al* (25) showed that adenoviral overexpression of FGF23 in rat calvarial cells *in vitro* inhibits bone mineralization independent of its systemic effects on phosphate homeostasis. We, and others, have also demonstrated that FGF23 treatment of primary calvarial osteoblast cultures from wild-type (WT) mice or from the osteoblastic MC3T3-E1 cell line leads to an inhibition of mineralization (21, 26), thus showing an effect on mineralization independent of circulating factors. The paradox of these findings inspired us to investigate the underlying mechanisms for the abnormal skeletal mineralization pattern seen in *Fgf23*$^{-/-}$ mice. We confirmed the accumulation of osteoid (osteoidosis) in the bone of these mice and discovered that expression of osteopontin (OPN), a well-known inhibitor of bone mineralization (27–30) is substantially elevated, suggesting a possible explanation for the improper mineralization of the bone. We now also demonstrate that ablation of *Opn* (*Spp1*) from *Fgf23*$^{-/-}$ mice, significantly ameliorates the osteomalacia. Collectively, these findings indicate that increased OPN levels are responsible, in part, for the skeletal mineralization defect seen in *Fgf23*$^{-/-}$ mice.

Material and Methods

Animals

Opn (Spp1)-knockout mice were obtained from the Jackson Laboratory (Bar Harbor, ME). Heterozygous *Fgf23*$^{+/-}$ animals were interbred with *Opn*$^{+/-}$ or *NaPi2a*$^{+/-}$ animals to obtain *Fgf23*$^{-/-}$/*Opn*$^{-/-}$ or *Fgf23*$^{-/-}$/*NaPi2a*$^{-/-}$ double-knockout mice for subsequent analyses.

Low-phosphate diet (0.17%) was obtained from PharmaServ Inc. (TestDiet, Cat#: 5857, Framingham, MA) and fed to the mice starting at 3-weeks of age for a duration of 3 weeks before collection of serum. The compound knockout *Fgf23*$^{-/-}$/*NaPi2a*$^{-/-}$ mice and the low-phosphate diet were used to examine the effects of phosphate and hypophosphatemia on *Opn* gene expression. The total body weight of each mouse was measured weekly starting at 3 weeks after birth. All animal procedures used were approved by the Institutional Animal Care and Use Committee at the Harvard Medical School.

Biochemical analyses

Blood was obtained by puncturing the cheek pouch of animals. Serum was isolated by centrifugation at 3000 g for 10 minutes and stored at − 80°C. Total serum calcium and phosphorus levels were determined using Stanbio LiquiColor (Arsenazo III) and LiquiUV kits (Stanbio Laboratory, Boerne, TX), respectively. Serum concentrations of OPN, CTX and 1,25$(OH)_2$D were measured using commercial ELISA kits from R&D Systems, Inc. (Minneapolis, MN) and IDS (Fountain Hills, AZ), respectively.

Bone histology, μCT analyses and histomorphometry

Micro-computed tomography (μCT) analysis was performed according to the recent guidelines (31) using a Scanco Medical μCT 35 system (Scanco, Southeastern, PA) with an isotropic voxel size of 7 μm to image the distal femur. For histomorphometry processing of undecalcified bone specimens and cancellous bone were performed as described previously (23). Femurs were fixed in 10% buffered formalin at 4°C overnight and stored in 70% ethanol at 4°C before being processed and embedded in methylmethacrylate. Three-μm-thick midsagittal sections of the distal femurs were prepared using a HM 360 microtome (Microm, Walldorf, Germany), and were stained with von Kossa/McNeal. Histomorphometric measurements in the distal femur were made on sections stained with von Kossa/McNeal using a semiautomatic system (OsteoMeasure, OsteoMetrics, Decatur, GA), and a Zeiss Axioskop microscope with a drawing attachment. The area within 0.25 mm from the growth plate was excluded from the measurements. All histomorphometric parameters were calculated and expressed according to the suggestions made by the ASBMR nomenclature committee (32).

In situ hybridization

Animals were dissected and tissues were fixed in 4% paraformaldehyde (PFA)/PBS pH 7.4 at 4°C for several days. Bones were subsequently demineralized for 1–2 weeks in 20% EDTA. All tissues were rinsed in PBS, dehydrated at room temperature through an ethanol series: 70% for 6 h, 80% for 1 h, 96% for 1 h and 100% for 3 h, cleared twice in xylene for 1 h/step, embedded in paraffin, serial sectioned at 6 μm using a Microm HM 360 microtome (Microm, Walldorf, Germany) and mounted on SuperFrost Plus slides. Complementary ^{35}S-UTP-labeled riboprobe OPN was used for performing *in situ* hybridization on paraffin sections, as described previously (33).

Immunohistochemistry

Immunohistochemistry was performed on paraffin sections using anti-mouse OPN antibody (R&D, Minneapolis, MN) with a working concentration of 0.5 μg/ml overnight at 4 °C. Non-immune immunoglobulin of the same isotype was used as a negative control. Tissue was stained with anti-goat HRP substrate and DAB (Vector, Burlingame, CA), and then counterstained with hematoxylin.

Quantitative real-time PCR

Total RNA from cortical bone of the femurs was extracted using Trizol reagent (Invitrogen, Carlsbad, CA) according to the manufacturer's protocol. For qRT-PCR, cDNA was prepared using QuantiTec reverse transcription kit (Qiagen, Valencia, CA) and analyzed with SYBR GreenMaster Mix (SABiosciences, Valencia, CA) in the iCycler (Bio-Rad, Hercules, CA) using specific primers designed for each targeted gene. Relative expression was calculated using the $2^{-\Delta\Delta Ct}$ method by normalizing with *Gapdh* housekeeping gene expression, and presented as fold increase relative to control.

Electron microscopy and immunolabeling of mouse bone sections for OPN

Calvariae from 3-wk-old *Fgf23*$^{-/-}$ and WT littermate mice were embedded in plastic for histology by light and transmission electron microscopy, and for high-resolution, immunogold ultrastructural labeling for OPN. Bones were fixed in 4% paraformaldehyde plus 1.0% glutaraldehyde in 0.1 M sodium cacodylate buffer, pH 7.3. Calvariae samples were left undecalcified for embedding in Epon epoxy resin (Cedarlane, Burlington, ON), or were decalcified for immunogold labeling in 8% EDTA over 2 weeks followed by embedding in LR White acrylic plastic (London Resin Company, Berkshire, UK). Samples destined for embedding in Epon for morphological analysis were additionally osmicated for 1 hour in potassium ferrocyanide-reduced 1% osmium tetroxide. Prior to embedding, all samples were dehydrated in a graded ethanol series, infiltrated with the embedding media, placed into mounting molds and the blocks were polymerized at 55°C for 2 days. For light microscopy, 1-μm-thick survey sections were cut from the polymerized blocks on a Leica Ultracut E ultramicrotome (Leica, Wetzlar, Germany) and stained for mineral by von Kossa staining (for the undecalcified samples) followed by counterstaining with toluidine blue. For light microscopy, sections were mounted on glass slides, cover-slipped, and viewed and photographed using a Leitz DMRBE (Leica, Wetzlar, Germany) optical microscope equipped with a 3-CCD Sony DXC-950 camera (Sony, Tokyo, Japan).

For transmission electron microscopy, 80-nm-thick sections were cut on the ultramicrotome followed by conventional staining with uranyl acetate and lead citrate after which the sections were viewed in a FEI Technai 12 transmission electron microscope (Hillsboro, OR) operating at 120 kV and equipped with a 792 Bioscan 1k × 1k wide-angle multiscan CCD camera (Pleasanton, CA). For immunogold labeling of OPN prior to transmission electron microscopy, LR White sections were incubated with polyclonal goat anti-mouse OPN antibody (R&D Systems, Minneapolis, MN), followed by rabbit anti-goat secondary antibody (Sigma Aldrich, St. Louis, MO), and then protein A-colloidal gold (14 nm) conjugate (Dr. G. Posthuma, University of Utrecht, Utrecht, The Netherlands).

Statistics

Statistically significant differences were evaluated by Student's t-test for comparison between two groups or by one-way analysis of variance (ANOVA) followed by the Tukey's test for multiple comparisons. All values are expressed as mean ± SD. A p value of less than 0.05 was considered to be statistically significant.

Results

Loss of FGF23 function results in a skeletal mineralization defect

Fig. 1A shows sections of undecalcified femurs obtained from 6-week-old *Fgf23*$^{-/-}$ and WT animals. Accumulation of osteoid (indicated by red arrows) is prominent in trabecular and cortical bone of *Fgf23*$^{-/-}$ animals. Comparison and quantification of the osteoid (osteoid over bone volume - OV/BV) showed a significant osteoid increase in the mutant mice

(55.8±11.5 %) when compared to that of control WT mice (2.6±0.9 %) (Fig. 1B). This observation was confirmed by the analyses of histology survey sections of undecalcified calvariae. The presence of thin osteoid seams in WT bone (Fig. 1C) is visible, but *Fgf23*$^{-/-}$ bone had large tracts of well-formed, but unmineralized bone in many locations. Upon closer inspection, even by light microscopy, this prominent osteoidosis in *Fgf23*$^{-/-}$ calvariae was unique in that a fine, speckled appearance was present (white boxes, right panel) in the widened osteoid. An ultrastructural investigation by transmission electron microscopy was made at these and other sites as indicated by the white boxes. This analysis revealed that the small speckles observed by light microscopy in *Fgf23*$^{-/-}$ bone were in fact numerous aborted mineralization foci in the widened osteoid seam that decreased in abundance towards the periosteal surface of the calvariae. While initial bone mineralization towards the endosteal surface proceeded in a seemingly normal manner to produce a thin continuous layer of mineralized bone, bulk mineralization of the *Fgf23*$^{-/-}$ bone matrix towards the periosteal surface terminated as a sharply defined border delimiting an aborted mineralization front.

There was a normal progression of bulk matrix mineralization to incorporate osteocytes into lacunae whose walls were well mineralized in WT calvarial bone. However, in *Fgf23*$^{-/-}$ calvariae, cells remaining as osteoid osteocytes in the widened osteoid seam were associated with a peculiar peripheral mineralization attempt characterized by finely granular mineral deposits surrounding the cells. This granular appearance again was reminiscent of aborted mineralization, which would otherwise be more confluent in appearance as in the wild-type bone surrounding osteocytes.

Increased OPN levels in *Fgf23*$^{-/-}$ mice

We investigated the expression of OPN, which is a well-recognized mineralization inhibitor (27–30), and found significantly elevated levels of this inhibitory protein in *Fgf23*$^{-/-}$ mice. Both *in situ* hybridization (Fig. 2A) and immunohistochemistry (Fig. 2B) were performed on femur sections of 6-week-old animals showing an enhanced OPN signal in bones of *Fgf23*$^{-/-}$ mice. This was confirmed by qRT-PCR analysis of cortical bones (femur), indicating that *Opn* mRNA levels in *Fgf23*$^{-/-}$ bone were 2-fold higher than in controls (Fig. 2C). Moreover, serum OPN levels in *Fgf23*$^{-/-}$ mice at 3 and 6 wks of age were 5.28±0.65 μg/ml and 4.42±1.41 μg/ml, respectively. These are over 13-fold higher than the levels in of controls (3 wk: 0.39±0.09 μg/ml; 6 wk: 0.28±0.14 μg/ml) (Fig. 2D).

Given its potency as a mineralization-inhibiting protein, we next investigated if there is an abnormal accumulation of OPN at these aborted mineralization sites in *Fgf23*$^{-/-}$ mice (Fig. 2E). Using the high-resolution immunogold staining method, we found intense labeling for OPN at levels well above those in WT bone at the aborted mineralization front, at the aborted mineralization foci in the widened osteoid seam, and at the edges of bone matrix surrounding the osteoid osteocytes. The locations correlate exactly with the sites described previously in Figure 1. Moreover, OPN derived at least in part locally from nearby osteocytes, as evidenced by secretory granule immune-gold labeling for OPN in these cells.

Deletion of *Opn* partially rescues the mineralization defect of *Fgf23*$^{-/-}$ mice

To investigate whether the increased OPN levels contribute to the skeletal mineralization defect in *Fgf23*$^{-/-}$ animals, we generated *Fgf23*$^{-/-}$/*Opn*$^{-/-}$ double-knockout mice *(DKO)* by interbreeding heterozygous *Fgf23*$^{+/-}$ and *Opn*$^{+/-}$ mice. *DKO* mice were more active, healthier and larger in size than *Fgf23*$^{-/-}$ littermates (Supplementary Fig. 1A). Their body weight was significantly higher than *Fgf23*$^{-/-}$ mice, although still lower than that of WT and *Opn*$^{-/-}$ mice (Supplementary Fig. 1B).

Biochemical assays of serum were performed for all four genotypes. No differences could be detected between the *Fgf23*$^{-/-}$ and *DKO* groups, with both being similarly hypercalcemic and hyperphosphatemic, and having significantly elevated serum 1,25 vitamin levels (Fig. 3).

We then performed μCT analyses and three-dimensional reconstruction of the bones to examine the skeletal phenotype of the mutant mice. Representative images of distal femoral metaphysis and midshaft cortex are shown in Figures 4A, C. Quantification of the μCT data demonstrated that the trabecular bone volume fraction (BV/TV) of the *Fgf23*$^{-/-}$ mice (2.0±1.3%) was significantly reduced compared to the other groups (Fig. 4B); it was restored in *DKO* mice (16.2±3.6%) to a volume exceeding that in *WT* (10.1±3.3%) and *Opn*$^{-/-}$ (14.2±3.2%) mice (Fig. 4B). Moreover, the thickness and architecture of the cortical bone were also significantly improved (Figs. 4C, D). As μCT analyzes only the mineralized part of the bone, these results indicate that the mineralization defect in these mice was partially rescued.

To further support our observation, we then performed histomorphometry of the trabecular area of the femora using undecalcified sections. We were able to confirm that BV/TV in the *DKO* bone was increased compared to that of *Fgf23*$^{-/-}$ (Fig. 5A & B). More importantly, the osteoidosis in the trabecular bone was markedly reduced in *DKO* bones (Fig. 5A). The osteoid volume (OV/BV) of the *DKO* mice (25.1±21.4%) was significantly lower than that of the *Fgf23*$^{-/-}$ mice (62.7±7.6%) (Fig. 5B). Similar changes were observed for the osteoid surface (OS/BS) and osteoid thickness (O.Th). Meanwhile, the mineralized bone volume (Md.V/TV) was significantly increased in *DKO* (Fig. 5B). In addition, the mineral apposition rate (MAR) in the *DKO*mice (1.9±0.3 μm/d) was completely restored to levels similar to the *WT* mice (2.6±0.7 μm/d). Moreover, there was no significant difference in the mineralization lag time (Mlt) when compared to the wild-type. In contrast, fluorochrome labeling of *Fgf23*$^{-/-}$ bones was generally indistinct and unsuccessful which we attribute to their prominent mineralization defect. Furthermore, osteoclast numbers (N.Oc/Md.Pm) were decreased in *DKO* mice as compared to *Fgf23*$^{-/-}$ mice (Fig. 5B). This was confirmed by the measurement of serum carboxy terminal cross-linked telopeptide of type I collagen (CTX), which showed that the increased level in *Fgf23*$^{-/-}$ mice was restored to a normal level in the *DKO* mice (Supplementary figure 2).

As shown in Figure 5C, the calvariae of the *Fgf23*$^{-/-}$ mice exhibited a widened osteoid. This was considerably reduced in the *DKO*, although some osteoidosis did persist. Breakthrough patches of mineralization were observed in the osteoid of the *DKO* mice, which indicates a partial recovery of mineralization in this widened osteoid seam (Fig. 5C).

Increased OPN levels were induced by the hyperphosphatemia

Fgf23$^{-/-}$ mice are severely hyperphosphatemic and we hypothesized that the increased OPN levels were induced by this hyperphosphatemia. We successfully reversed the serum phosphate levels in *Fgf23*$^{-/-}$ mice by generating *Fgf23*$^{-/-}$/*NaPi2a*$^{-/-}$ double-knockout mice and by feeding *Fgf23*$^{-/-}$ mice a low-phosphate diet. In both cases, the serum phosphate levels were significantly lower than those of *WT* and *Fgf23*$^{-/-}$ mice (Fig. 6A). We also found that the OPN levels in *Fgf23*$^{-/-}$ mice were significantly decreased when serum phosphate levels were lowered, although they remained significantly higher than in controls (Fig. 6B). These data indicate that phosphate is an important contributor to the high OPN levels in *Fgf23*$^{-/-}$ mice. Low-phosphate diet feeding also led to a partial decrease of OPN in *WT* mice, while it remained unchanged in *NaPi2a*$^{-/-}$ mice.

Discussion

Renal phosphate wasting typically leads to hypophosphatemia and osteomalacia. However, *Fgf23*$^{-/-}$ mice having a severe osteomalacic mineralization defect paradoxically have hyperphosphatemia (and hypercalcemia). Here, we have demonstrated that *Fgf23*$^{-/-}$ mice have greatly elevated *Opn* gene expression and OPN protein accumulation in bone, and also highly elevated serum OPN. Our experiments that reduced serum phosphate levels by dietary and genetic means demonstrated that the increase in OPN in the *Fgf23*$^{-/-}$ mice was caused at least in part by higher circulating phosphate. Furthermore, we have shown that deletion of *Opn* from *Fgf23*$^{-/-}$ mice partially rescues the mineralization defect such that the osteomalacia is significantly reduced. Taken together, these data suggest that increased OPN levels are at least in part responsible for the skeletal mineralization defect observed in *Fgf23*$^{-/-}$ mice.

OPN, also originally known as secreted phosphoprotein 1 (SPP1), is a member of the SIBLING family (small integrin-binding ligands N-linked glycoproteins) of extracellular matrix mineral-binding proteins (34–36). In bone, OPN is produced abundantly by osteoblasts and osteocytes as a phosphorylated, secreted extracellular matrix protein (37, 38). Once in the extracellular matrix, OPN binds avidly to mineral crystal surfaces (39–42) to inhibit their growth as it loads into the bulk phase of the mineralizing bone matrix. Within the extracellular matrix of bone, enzymatic degradation of OPN by PHEX (phosphate-regulating gene with homologies to endopeptidases on the X-chromosome) and removal of phosphates by TNAP (tissue-nonspecific alkaline phosphatase, ALPL) may modulate the mineralization-inhibiting activities of this protein (28, 29, 43, 44). OPN also accumulates at cell- and matrix-matrix interfaces where mineralization is tightly controlled such as at cement lines and at the lamina limitans found at the osteocyte- and bone-lining cell-matrix interface where mineralization is essentially terminated, presumably via the actions of the accumulated inhibitory OPN at these interfacial sites (45), while not excluding similar inhibitory functions by other proteins/peptides at these same locations. Besides non-collagenous proteins, mineralization may likewise be partly regulated in the extracellular matrix by collagen itself and its processing by enzymes (46).

Amongst myriad functions shown for OPN (27, 47, 48), one of its most prominent functions includes direct inhibition of hydroxyapatite crystal growth by binding to lattice calcium exposed at crystal surfaces, regulating crystal dimensions by limiting growth where it has bound (49, 50). Its high negative charge derived primarily from abundant aspartic acid and glutamic acid amino acid residues, along with it having a high level of post-translational phosphorylation, all lead to an extended and flexible protein capable of binding positively charged calcium atoms residing at crystal surfaces (51, 52). Proteins binding in this way to bio-minerals generally act as inhibitors, influencing the number, form, shape and alignment of the mineral crystals (53) in bones and teeth, mineral crystal growth takes place in the collagenous extracellular matrix permeated by numerous noncollagenous proteins and small proteoglycans thought to regulate the mineralization process within the collagen scaffold. OPN is the most widely studied protein within the SIBLING family of bone and tooth noncollagenous proteins, and its properties as a mineralization inhibitor appear to be far greater than the other SIBLING proteins (54). OPN is upregulated locally and accumulates at high levels at sites of ectopic calcification where it is thought to be involved in the host response to limit this pathologic mineralization (55, 56); indeed, deletion of OPN from matrix Gla protein (MGP)-deficient mice showing severe vascular calcification leads to increased vascular calcification and even earlier mortality (57). As another example, OPN-deficient mice are also prone to kidney stone formation (58). OPN also interplays with the other members of SIBLING family. For example, OPN protein expression in bone is dramatically decreased in MEPE overexpressing mice (59).

For bone, OPN-deficient mice show increased mineralization (60) coincident with reduced bone biomechanical properties (61). In recent years, several knockout mouse models have been shown to exhibit elevated OPN that has been suggested to contribute to the osteomalacic phenotype (62, 63). Also of importance in determining OPN levels in the bone is the observation that OPN and its peptides (including the ASARM peptide) can be inactivated by their essentially complete degradation by the enzyme PHEX (29, 43), thus explaining the accumulation of OPN and OPN fragments in the Hyp mouse model of X-linked hypophosphatemia, a human disease with inactivating mutations in PHEX leading to renal phosphate wasting, hypophosphatemia and osteomalacia.

In the present study, we demonstrated that the elevated OPN levels seen in the *Fgf23*$^{-/-}$ mice were significantly decreased when serum phosphate levels were lowered – either through diet or deletion of renal phosphate co-transporter activity – indicating that the hyperphosphatemia in *Fgf23*$^{-/-}$ mice is at least in part responsible for the increased OPN levels. Indeed, phosphate is not only a potent regulator of mineralization, but it acts as a specific signal for induction of *Opn* expression in osteoblast lineage cells (64, 65). This latter effect requires the activity of ERK1/2 and protein kinase C, as well as the glucocorticoid receptor and proteosomal/ubiquination pathways (65, 66). Phosphate also induces the expression of *Opn* in vascular smooth muscle cells relevant to the frequency with which vascular calcification is observed (67). In contrast, however, we have previously reported that mice deficient for both KLOTHO and PTH, which exhibit extremely high serum phosphate levels, have normal OPN expression and serum levels (68) accompanied by normal bone mineralization. PTH is another known regulator of *Opn*, which increases its transcription and expression in osteoblasts (69, 70); accordingly, this loss of PTH induction of OPN could offset the effect of the high serum phosphate in these mice in terms of modulating OPN levels. Related to these findings, we observed that PTH levels in *Fgf23*$^{-/-}$ mice were low-to-undetectable (2, 21), eliminating this PTH-induction pathway option as a potential explanation for the high OPN levels. In addition, even genetic deletion of PTH from *Fgf23*$^{-/-}$ mice did not affect the increased OPN level (68) or rescue the skeletal mineralization defects (24), again suggesting that PTH is not a key factor responsible for the increased OPN level observed in *Fgf23*$^{-/-}$ mice.

In terms of vitamin D regulation, $1,25(OH)_2D$ is known to induce gene expression of *Opn* via binding of the VDRE (vitamin D response element) to regulatory sequences directly upstream of the *Opn* promoter (71). Lieben *et al*. (72) demonstrated that $1,25(OH)_2D$ suppresses mineralization by upregulating *Opn* expression and PPi levels. Our previous study also showed that ablation of vitamin D signaling rescues bone and mineral homeostasis in *Fgf23*$^{-/-}$ mice fed a high-calcium and high-phosphate diet (73). To investigate whether the elevated serum levels of $1,25(OH)_2D$ are another potential explanation for the high OPN levels in *Fgf23*$^{-/-}$ mice, we eliminated all vitamin D signaling by genetic deletion of *1a(OH)ase* from *Fgf23*$^{-/-}$ mice (*Fgf23*$^{-/-}$/*1a(OH)ase*$^{-/-}$). This deletion did not change the increased OPN levels, suggesting that vitamin D is not responsible for the elevated OPN level observed in *Fgf23*$^{-/-}$ mice (Supplementary Figure 3).

Transmission electron microscopy was used to examine the inhibited mineralization process and the cellular secretion and accumulation of OPN in *Fgf23*$^{-/-}$ mice at the ultrastructural level. Inhibited mineralization appeared to reside at three locations within the bone matrix, with each inhibited site showing an abundant accumulation of OPN as detected by immunogold labeling. These sites where mineralization was inhibited, and possibly even completely aborted, included small punctate foci throughout the osteoid, a pericellular rim of matrix/mineral at the margins of osteocyte lacunae, and a generally sharply defined mineralization front separating the osteoid from the mineralized bone matrix proper. The tissue morphology at these locations indicates interruption of normal mineralization

pathways, which together with the excessive accumulation of OPN at these sites which otherwise show much lesser OPN accumulation in normal WT mice at similar sites (45), all indicate that the mechanism of this inhibition resides in OPN's mineral-binding and inhibitory function. Normally, OPN is thought to regulate crystal growth as it occurs in the bulk bone matrix at small mineralization foci and at the mineralization front, and surrounding osteocytes where mineralization has to be terminated to maintain the patency of osteocyte lacunae. Indeed, in the *Fgf23*$^{-/-}$ mice, OPN was found at its highest levels to inhibit mineralization precisely at these same locations where regulation/inhibition of mineralization is normally ongoing, and removing OPN in FGF23-deficient mice in the double knockout (*Fgf23*$^{-/-}$/*Opn*$^{-/-}$) partially rescued this inhibition.

In addition to advances made in recent years in understanding the roles of phosphorylated SIBLING proteins (and functionally active peptides derived from them) in modulating mineralization, similar progress has been made towards understanding the role of pyrophosphate (PPi) in inhibiting mineralization. In both cases – for proteins and PPi – processing enzymes play key roles in inactivating and activating these molecular determinants of mineralization, as shown by the consequences (osteomalacia) of inactivating mutations in *ALPL* affecting PPi degradation (hypophosphatasia) (74), and in *PHEX* affecting OPN degradation (X-linked hypophosphatemia) (75), where PPi and OPN respectively accumulate in the bone matrix to inhibit mineralization. Elegant genetic studies in mice by Millan and colleagues have also clearly shown the combined action of these two determinants to modulate the P:PPi ratio and to elevate inhibitory OPN protein levels (63), both of which may simultaneously contribute to osteomalacia where serum phosphate and calcium levels are within the normal range. Such inhibition of bone mineralization – unlike the systemic effects of renal phosphate wasting – is thought to occur locally at the level of the extracellular matrix, and for OPN, phosphorylation status appears to be particularly important (29, 44, 50, 76, 77). Indeed, phosphorylated OPN may be a more potent inhibitor than PPi *in vivo* given that elevated extracellular PPi levels found in *Opn*$^{-/-}$ mice did not cause osteomalacia (62, 63), where it was proposed that much higher levels of PPi might be needed in the absence of OPN to affect mineralization. Here, in the present study, we provide new evidence in another genetic mouse model (*Fgf23*$^{-/-}$) for this local matrix mineralization inhibitory effect of OPN, and we additionally show by immunogold labeling the ultrastructural accumulation of OPN in the extracellular matrix at precisely the sites where matrix mineralization is inhibited. Taken together, these findings demonstrate that apart from the well-known effects on skeletal mineralization of changes in systemic phosphate and calcium homeostasis, that there exists another level of potent regulation at the local level residing within the activities of the noncollagenous proteins of the extracellular matrix – most notably that of OPN.

Supplementary Material

Refer to Web version on PubMed Central for supplementary material.

Acknowledgments

This work was supported by grants from the National Institute of Diabetes and Digestive and Kidney Diseases (NIDDK) R01-073944 to BL, and from the Canadian Institutes of Health Research (CIHR) MOP97858 to MDM, and from Natural Science Foundation of China (30901696) and Program for New Century Excellent Talents in University (NCET-12-0379) to QY. MDM is a member of the FRQ-S Groupe de Recherche Axé sur la Structure des Protéines, the FRQ-S Réseau de Recherche en Santé Buccodentaire et Osseuse, and the McGill Centre for Bone and Periodontal Research.

Disclosure section:

MDM has received research grants from, and served as a consultant for, Enobia Pharma (now Alexion Pharmaceuticals).

References

1. Shimada T, Kakitani M, Yamazaki Y, Hasegawa H, Takeuchi Y, Fujita T, et al. Targeted ablation of Fgf23 demonstrates an essential physiological role of FGF23 in phosphate and vitamin D metabolism. The Journal of clinical investigation. 2004; 113(4):561–568. Epub 2004/02/18. [PubMed: 14966565]
2. Sitara D, Razzaque MS, Hesse M, Yoganathan S, Taguchi T, Erben RG, et al. Homozygous ablation of fibroblast growth factor-23 results in hyperphosphatemia and impaired skeletogenesis, and reverses hypophosphatemia in Phex-deficient mice. Matrix Biol. 2004; 23(7):421–432. [PubMed: 15579309]
3. Bergwitz C, Juppner H. Regulation of phosphate homeostasis by PTH, vitamin D, and FGF23. Annu Rev Med. 2010; 61:91–104. Epub 2010/01/12. [PubMed: 20059333]
4. ADHR Consortium. Autosomal dominant hypophosphataemic rickets is associated with mutations in FGF23. The ADHR Consortium. Nat Genet. 2000; 26(3):345–348. [PubMed: 11062477]
5. Autosomal dominant hypophosphataemic rickets is associated with mutations in FGF23. Nat Genet. 2000; 26(3):345–348. Epub 2000/11/04. [PubMed: 11062477]
6. The HYP Consortium. A gene (PEX) with homologies to endopeptidases is mutated in patients with X-linked hypophosphatemic rickets. Nat Genet. 1995; 11(2):130–136. Epub 1995/10/01. [PubMed: 7550339]
7. Nelson AE, Hogan JJ, Holm IA, Robinson BG, Mason RS. Phosphate wasting in oncogenic osteomalacia: PHEX is normal and the tumor-derived factor has unique properties. Bone. 2001; 28(4):430–439. [PubMed: 11336925]
8. Larsson T, Nisbeth U, Ljunggren O, Juppner H, Jonsson KB. Circulating concentration of FGF-23 increases as renal function declines in patients with chronic kidney disease, but does not change in response to variation in phosphate intake in healthy volunteers. Kidney Int. 2003; 64(6):2272–2279. Epub 2003/11/25. [PubMed: 14633152]
9. Larsson T, Yu X, Davis SI, Draman MS, Mooney SD, Cullen MJ, et al. A novel recessive mutation in fibroblast growth factor-23 causes familial tumoral calcinosis. The Journal of clinical endocrinology and metabolism. 2005; 90(4):2424–2427. Epub 2005/02/03. [PubMed: 15687325]
10. Kobayashi K, Imanishi Y, Koshiyama H, Miyauchi A, Wakasa K, Kawata T, et al. Expression of FGF23 is correlated with serum phosphate level in isolated fibrous dysplasia. Life Sci. 2006; 78(20):2295–2301. Epub 2005/12/13. [PubMed: 16337659]
11. Riminucci M, Collins MT, Fedarko NS, Cherman N, Corsi A, White KE, et al. FGF-23 in fibrous dysplasia of bone and its relationship to renal phosphate wasting. The Journal of clinical investigation. 2003; 112(5):683–692. Epub 2003/09/04. [PubMed: 12952917]
12. Yoshiko Y, Wang H, Minamizaki T, Ijuin C, Yamamoto R, Suemune S, et al. Mineralized tissue cells are a principal source of FGF23. Bone. 2007; 40(6):1565–1573. Epub 2007/03/14. [PubMed: 17350357]
13. Mirams M, Robinson BG, Mason RS, Nelson AE. Bone as a source of FGF23: regulation by phosphate? Bone. 2004; 35(5):1192–1199. [PubMed: 15542045]
14. Kurosu H, Ogawa Y, Miyoshi M, Yamamoto M, Nandi A, Rosenblatt KP, et al. Regulation of fibroblast growth factor-23 signaling by Klotho. J Biol Chem. 2006
15. Urakawa I, Yamazaki Y, Shimada T, Iijima K, Hasegawa H, Okawa K, et al. Klotho converts canonical FGF receptor into a specific receptor for FGF23. Nature. 2006
16. Tomiyama K, Maeda R, Urakawa I, Yamazaki Y, Tanaka T, Ito S, et al. Relevant use of Klotho in FGF19 subfamily signaling system in vivo. Proc Natl Acad Sci U S A. 2010; 107(4):1666–1671. Epub 2010/01/19. [PubMed: 20080590]
17. Saito H, Kusano K, Kinosaki M, Ito H, Hirata M, Segawa H, et al. Human fibroblast growth factor-23 mutants suppress Na+-dependent phosphate co-transport activity and 1alpha,25-dihydroxyvitamin D3 production. J Biol Chem. 2003; 278(4):2206–2211. Epub 2002/11/07. [PubMed: 12419819]

18. Shimada T, Urakawa I, Yamazaki Y, Hasegawa H, Hino R, Yoneya T, et al. FGF-23 transgenic mice demonstrate hypophosphatemic rickets with reduced expression of sodium phosphate cotransporter type IIa. Biochem Biophys Res Commun. 2004; 314(2):409–414. Epub 2004/01/22. [PubMed: 14733920]
19. Bai X, Miao D, Li J, Goltzman D, Karaplis AC. Transgenic mice overexpressing human fibroblast growth factor 23 (R176Q) delineate a putative role for parathyroid hormone in renal phosphate wasting disorders. Endocrinology. 2004; 145(11):5269–5279. Epub 2004/07/31. [PubMed: 15284207]
20. Sitara D, Razzaque MS, St-Arnaud R, Huang W, Taguchi T, Erben RG, et al. Genetic ablation of vitamin D activation pathway reverses biochemical and skeletal anomalies in Fgf-23-null animals. Am J Pathol. 2006; 169(6):2161–2170. Epub 2006/12/07. [PubMed: 17148678]
21. Sitara D, Kim S, Razzaque MS, Bergwitz C, Taguchi T, Schuler C, et al. Genetic evidence of serum phosphate-independent functions of FGF-23 on bone. PLoS Genet. 2008; 4(8):e1000154. Epub 2008/08/09. [PubMed: 18688277]
22. Razzaque MS, Sitara D, Taguchi T, St-Arnaud R, Lanske B. Premature ageing-like phenotype in fibroblast growth factor 23 null mice is a vitamin-D mediated process. The FASEB Journal. 2006; 20(6):720–722.
23. Yuan Q, Sato T, Densmore M, Saito H, Schuler C, Erben RG, et al. Fgf23/Klotho signaling is not essential for the phosphaturic and anabolic functions of PTH. Journal of bone and mineral research : the official journal of the American Society for Bone and Mineral Research. 2011; 26(9):2026–2035. Epub 2011/05/19. [PubMed: 21590742]
24. Yuan Q, Sitara D, Sato T, Densmore M, Saito H, Schuler C, et al. PTH Ablation Ameliorates the Anomalies of Fgf23-Deficient Mice by Suppressing the Elevated Vitamin D and Calcium Levels. Endocrinology. 2011; 152(11):4053–4061. Epub 2011/09/08. [PubMed: 21896668]
25. Wang H, Yoshiko Y, Yamamoto R, Minamizaki T, Kozai K, Tanne K, et al. Overexpression of fibroblast growth factor 23 suppresses osteoblast differentiation and matrix mineralization in vitro. Journal of bone and mineral research : the official journal of the American Society for Bone and Mineral Research. 2008; 23(6):939–948. Epub 2008/02/20. [PubMed: 18282132]
26. Shalhoub V, Ward SC, Sun B, Stevens J, Renshaw L, Hawkins N, et al. Fibroblast growth factor 23 (FGF23) and alpha-klotho stimulate osteoblastic MC3T3.E1 cell proliferation and inhibit mineralization. Calcif Tissue Int. 2011; 89(2):140–150. Epub 2011/06/03. [PubMed: 21633782]
27. Sodek J, Ganss B, McKee MD. Osteopontin. Crit Rev Oral Biol Med. 2000; 11(3):279–303. Epub 2000/10/06. [PubMed: 11021631]
28. Addison WN, Azari F, Sorensen ES, Kaartinen MT, McKee MD. Pyrophosphate inhibits mineralization of osteoblast cultures by binding to mineral, up-regulating osteopontin, and inhibiting alkaline phosphatase activity. J Biol Chem. 2007; 282(21):15872–15883. Epub 2007/03/27. [PubMed: 17383965]
29. Addison WN, Masica DL, Gray JJ, McKee MD. Phosphorylation-dependent inhibition of mineralization by osteopontin ASARM peptides is regulated by PHEX cleavage. Journal of bone and mineral research : the official journal of the American Society for Bone and Mineral Research. 2010; 25(4):695–705. Epub 2009/09/25. [PubMed: 19775205]
30. Gericke A, Qin C, Spevak L, Fujimoto Y, Butler WT, Sorensen ES, et al. Importance of phosphorylation for osteopontin regulation of biomineralization. Calcif Tissue Int. 2005; 77(1):45–54. Epub 2005/07/12. [PubMed: 16007483]
31. Bouxsein ML, Boyd SK, Christiansen BA, Guldberg RE, Jepsen KJ, Muller R. Guidelines for assessment of bone microstructure in rodents using micro-computed tomography. Journal of bone and mineral research : the official journal of the American Society for Bone and Mineral Research. 2010; 25(7):1468–1486. Epub 2010/06/10. [PubMed: 20533309]
32. Dempster DW, Compston JE, Drezner MK, Glorieux FH, Kanis JA, Malluche H, et al. Standardized nomenclature, symbols, and units for bone histomorphometry: a 2012 update of the report of the ASBMR Histomorphometry Nomenclature Committee. Journal of bone and mineral research : the official journal of the American Society for Bone and Mineral Research. 2013; 28(1):2–17. Epub 2012/12/01. [PubMed: 23197339]

33. Lanske B, Divieti P, Kovacs CS, Pirro A, Landis WJ, Krane SM, et al. The parathyroid hormone (PTH)/PTH-related peptide receptor mediates actions of both ligands in murine bone. Endocrinology. 1998; 139(12):5194–5204. [PubMed: 9832460]
34. Fisher LW, Fedarko NS. Six genes expressed in bones and teeth encode the current members of the SIBLING family of proteins. Connect Tissue Res. 2003; 44(Suppl 1):33–40. Epub 2003/09/04. [PubMed: 12952171]
35. Staines KA, MacRae VE, Farquharson C. The importance of the SIBLING family of proteins on skeletal mineralisation and bone remodelling. J Endocrinol. 2012; 214(3):241–255. Epub 2012/06/16. [PubMed: 22700194]
36. Rowe PS. The chicken or the egg: PHEX, FGF23 and SIBLINGs unscrambled. Cell Bio chem Funct. 2012; 30(5):355–375. Epub 2012/05/11.
37. Zohar R, Lee W, Arora P, Cheifetz S, McCulloch C, Sodek J. Single cell analysis of intracellular osteopontin in osteogenic cultures of fetal rat calvarial cells. Journal of cellular physiology. 1997; 170(1):88–100. Epub 1997/01/01. [PubMed: 9012788]
38. Dodds RA, Connor JR, James IE, Rykaczewski EL, Appelbaum E, Dul E, et al. Human osteoclasts, not osteoblasts, deposit osteopontin onto resorption surfaces: an in vitro and ex vivo study of remodeling bone. Journal of bone and mineral research : the official journal of the American Society for Bone and Mineral Research. 1995; 10(11):1666–1680. Epub 1995/11/01. [PubMed: 8592943]
39. McKee MD, Glimcher MJ, Nanci A. High-resolution immunolocalization of osteopontin and osteocalcin in bone and cartilage during endochondral ossification in the chicken tibia. Anat Rec. 1992; 234(4):479–492. Epub 1992/12/01. [PubMed: 1456451]
40. McKee MD, Farach-Carson MC, Butler WT, Hauschka PV, Nanci A. Ultrastructural immunolocalization of noncollagenous (osteopontin and osteocalcin) and plasma (albumin and alpha 2HS-glycoprotein) proteins in rat bone. Journal of bone and mineral research : the official journal of the American Society for Bone and Mineral Research. 1993; 8(4):485–496. Epub 1993/04/01. [PubMed: 8475798]
41. Hunter GK, Kyle CL, Goldberg HA. Modulation of crystal formation by bone phosphoproteins: structural specificity of the osteopontin-mediated inhibition of hydroxyapatite formation. Bio chem J. 1994; 300(Pt 3):723–728. Epub 1994/06/15.
42. Boskey AL, Maresca M, Ullrich W, Doty SB, Butler WT, Prince CW. Osteopontin-hydroxyapatite interactions in vitro: inhibition of hydroxyapatite formation and growth in a gelatin-gel. Bone Miner. 1993; 22(2):147–159. Epub 1993/08/01. [PubMed: 8251766]
43. Barros NM, Hoac B, Neves RL, Addison WN, Assis DM, Murshed M, et al. Proteolytic processing of osteopontin by PHEX and accumulation of osteopontin fragments in Hyp mouse bone, the murine model of X-linked hypophosphatemia. Journal of bone and mineral research : the official journal of the American Society for Bone and Mineral Research. 2013; 28(3):688–699. Epub 2012/09/20. [PubMed: 22991293]
44. Narisawa S, Yadav MC, Millan JL. In vivo overexpression of tissue-nonspecific alkaline phosphatase increases skeletal mineralization and affects the phosphorylation status of osteopontin. Journal of bone and mineral research : the official journal of the American Society for Bone and Mineral Research. 2013 Epub 2013/02/22.
45. McKee MD, Nanci A. Osteopontin at mineralized tissue interfaces in bone, teeth, and osseointegrated implants: ultrastructural distribution and implications for mineralized tissue formation, turnover, and repair. Microsc Res Tech. 1996; 33(2):141–164. Epub 1996/02/01. [PubMed: 8845514]
46. Holmbeck K, Bianco P, Yamada S, Birkedal-Hansen H. MT1-MMP: a tethered collagenase. Journal of cellular physiology. 2004; 200(1):11–19. Epub 2004/05/12. [PubMed: 15137053]
47. Scatena M, Liaw L, Giachelli CM. Osteopontin: a multifunctional molecule regulating chronic inflammation and vascular disease. Arterioscler Thromb Vasc Biol. 2007; 27(11):2302–2309. Epub 2007/08/25. [PubMed: 17717292]
48. Wang KX, Denhardt DT. Osteopontin: role in immune regulation and stress responses. Cytokine Growth Factor Rev. 2008; 19(5–6):333–345. Epub 2008/10/28. [PubMed: 18952487]

49. Steitz SA, Speer MY, McKee MD, Liaw L, Almeida M, Yang H, et al. Osteopontin inhibits mineral deposition and promotes regression of ectopic calcification. The American journal of pathology. 2002; 161(6):2035–2046. Epub 2002/12/06. [PubMed: 12466120]
50. Pampena DA, Robertson KA, Litvinova O, Lajoie G, Goldberg HA, Hunter GK. Inhibition of hydroxyapatite formation by osteopontin phosphopeptides. Biochem J. 2004; 378(Pt 3):1083–1087. Epub 2003/12/18. [PubMed: 14678013]
51. Hunter GK, O'Young J, Grohe B, Karttunen M, Goldberg HA. The flexible polyelectrolyte hypothesis of protein-biomineral interaction. Langmuir. 2010; 26(24):18639–18646. Epub 2010/06/10. [PubMed: 20527831]
52. Azzopardi PV, O'Young J, Lajoie G, Karttunen M, Goldberg HA, Hunter GK. Roles of electrostatics and conformation in protein-crystal interactions. PLoS One. 2010; 5(2):e9330. Epub 2010/02/23. [PubMed: 20174473]
53. McKee MD, Addison WN, Kaartinen MT. Hierarchies of extracellular matrix and mineral organization in bone of the craniofacial complex and skeleton. Cells Tissues Organs. 2005; 181(3–4):176–188. Epub 2006/04/14. [PubMed: 16612083]
54. Goldberg HA, Warner KJ, Li MC, Hunter GK. Binding of bone sialoprotein, osteopontin and synthetic polypeptides to hydroxyapatite. Connect Tissue Res. 2001; 42(1):25–37. Epub 2001/11/08. [PubMed: 11696986]
55. Jahnen-Dechent W, Schafer C, Ketteler M, McKee MD. Mineral chaperones: a role for fetuin-A and osteopontin in the inhibition and regression of pathologic calcification. J Mol Med (Berl). 2008; 86(4):379–389. Epub 2007/12/18. [PubMed: 18080808]
56. Giachelli CM. Ectopic calcification: new concepts in cellular regulation. Z Kardiol. 2001; 90(Suppl 3):31–37. Epub 2001/05/26. [PubMed: 11374030]
57. Speer MY, McKee MD, Guldberg RE, Liaw L, Yang HY, Tung E, et al. Inactivation of the osteopontin gene enhances vascular calcification of matrix Gla protein-deficient mice: evidence for osteopontin as an inducible inhibitor of vascular calcification in vivo. J Exp Med. 2002; 196(8):1047–1055. Epub 2002/10/23. [PubMed: 12391016]
58. Mo L, Liaw L, Evan AP, Sommer AJ, Lieske JC, Wu XR. Renal calcinosis and stone formation in mice lacking osteopontin, Tamm-Horsfall protein, or both. Am J Physiol Renal Physiol. 2007; 293(6):F1935–F1943. Epub 2007/09/28. [PubMed: 17898038]
59. David V, Martin A, Hedge AM, Rowe PS. Matrix extracellular phosphoglycoprotein (MEPE) is a new bone renal hormone and vascularization modulator. Endocrinology. 2009; 150(9):4012–4023. Epub 2009/06/13. [PubMed: 19520780]
60. Boskey AL, Spevak L, Paschalis E, Doty SB, McKee MD. Osteopontin deficiency increases mineral content and mineral crystallinity in mouse bone. Calcif Tissue Int. 2002; 71(2):145–154. Epub 2002/06/20. [PubMed: 12073157]
61. Thurner PJ, Chen CG, Ionova-Martin S, Sun L, Harman A, Porter A, et al. Osteopontin deficiency increases bone fragility but preserves bone mass. Bone. 2010; 46(6):1564–1573. Epub 2010/02/23. [PubMed: 20171304]
62. Harmey D, Hessle L, Narisawa S, Johnson KA, Terkeltaub R, Millan JL. Concerted regulation of inorganic pyrophosphate and osteopontin by akp2, enpp1, and ank: an integrated model of the pathogenesis of mineralization disorders. The American journal of pathology. 2004; 164(4):1199–1209. Epub 2004/03/25. [PubMed: 15039209]
63. Harmey D, Johnson KA, Zelken J, Camacho NP, Hoylaerts MF, Noda M, et al. Elevated skeletal osteopontin levels contribute to the hypophosphatasia phenotype in Akp2(−/−) mice. Journal of bone and mineral research : the official journal of the American Society for Bone and Mineral Research. 2006; 21(9):1377–1386. Epub 2006/08/31. [PubMed: 16939396]
64. Rutherford RB, Foster BL, Bammler T, Beyer RP, Sato S, Somerman MJ. Extracellular phosphate alters cementoblast gene expression. J Dent Res. 2006; 85(6):505–509. Epub 2006/05/26. [PubMed: 16723645]
65. Fatherazi S, Matsa-Dunn D, Foster BL, Rutherford RB, Somerman MJ, Presland RB. Phosphate regulates osteopontin gene transcription. J Dent Res. 2009; 88(1):39–44. Epub 2009/01/10. [PubMed: 19131315]

66. Beck GR Jr, Knecht N. Osteopontin regulation by inorganic phosphate is ERK1/2-, protein kinase C-, and proteasome-dependent. J Biol Chem. 2003; 278(43):41921–41929. Epub 2003/08/16. [PubMed: 12920127]

67. El-Abbadi MM, Pai AS, Leaf EM, Yang HY, Bartley BA, Quan KK, et al. Phosphate feeding induces arterial medial calcification in uremic mice: role of serum phosphorus, fibroblast growth factor-23, and osteopontin. Kidney Int. 2009; 75(12):1297–1307. Epub 2009/03/27. [PubMed: 19322138]

68. Yuan Q, Sato T, Densmore M, Saito H, Schuler C, Erben RG, et al. Deletion of PTH rescues skeletal abnormalities and high osteopontin levels in Klotho−/− mice. PLoS Genet. 2012; 8(5):e1002726. Epub 2012/05/23. [PubMed: 22615584]

69. Noda M, Rodan GA. Transcriptional regulation of osteopontin production in rat osteoblast-like cells by parathyroid hormone. J Cell Biol. 1989; 108(2):713–718. Epub 1989/02/01. [PubMed: 2465299]

70. Gopalakrishnan R, Ouyang H, Somerman MJ, McCauley LK, Franceschi RT. Matrix gamma-carboxyglutamic acid protein is a key regulator of PTH-mediated inhibition of mineralization in MC3T3-E1 osteoblast-like cells. Endocrinology. 2001; 142(10):4379–4388. Epub 2001/09/21. [PubMed: 11564701]

71. Meyer MB, Goetsch PD, Pike JW. Genome-wide analysis of the VDR/RXR cistrome in osteoblast cells provides new mechanistic insight into the actions of the vitamin D hormone. J Steroid Biochem Mol Biol. 2010; 121(1–2):136–141. Epub 2010/02/23. [PubMed: 20171278]

72. Lieben L, Masuyama R, Torrekens S, Van Looveren R, Schrooten J, Baatsen P, et al. Normocalcemia is maintained in mice under conditions of calcium malabsorption by vitamin D-induced inhibition of bone mineralization. J Clin Invest. 2012; 122(5):1803–1815. Epub 2012/04/24. [PubMed: 22523068]

73. Hesse M, Frohlich LF, Zeitz U, Lanske B, Erben RG. Ablation of vitamin D signaling rescues bone, mineral, and glucose homeostasis in Fgf-23 deficient mice. Matrix biology : journal of the International Society for Matrix Biology. 2007; 26(2):75–84. Epub 2006/11/25. [PubMed: 17123805]

74. Whyte MP. Physiological role of alkaline phosphatase explored in hypophosphatasia. Ann N Y Acad Sci. 2010; 1192:190–200. Epub 2010/04/16. [PubMed: 20392236]

75. Carpenter TO. The expanding family of hypophosphatemic syndromes. J Bone Miner Metab. 2011; 30(1):1–9. Epub 2011/12/15. [PubMed: 22167381]

76. Tagliabracci VS, Engel JL, Wen J, Wiley SE, Worby CA, Kinch LN, et al. Secreted kinase phosphorylates extracellular proteins that regulate biomineralization. Science. 2012; 336(6085): 1150–1153. Epub 2012/05/15. [PubMed: 22582013]

77. Boskey AL, Christensen B, Taleb H, Sorensen ES. Post-translational modification of osteopontin: effects on in vitro hydroxyapatite formation and growth. Biochem Biophys Res Commun. 2012; 419(2):333–338. Epub 2012/02/22. [PubMed: 22342723]

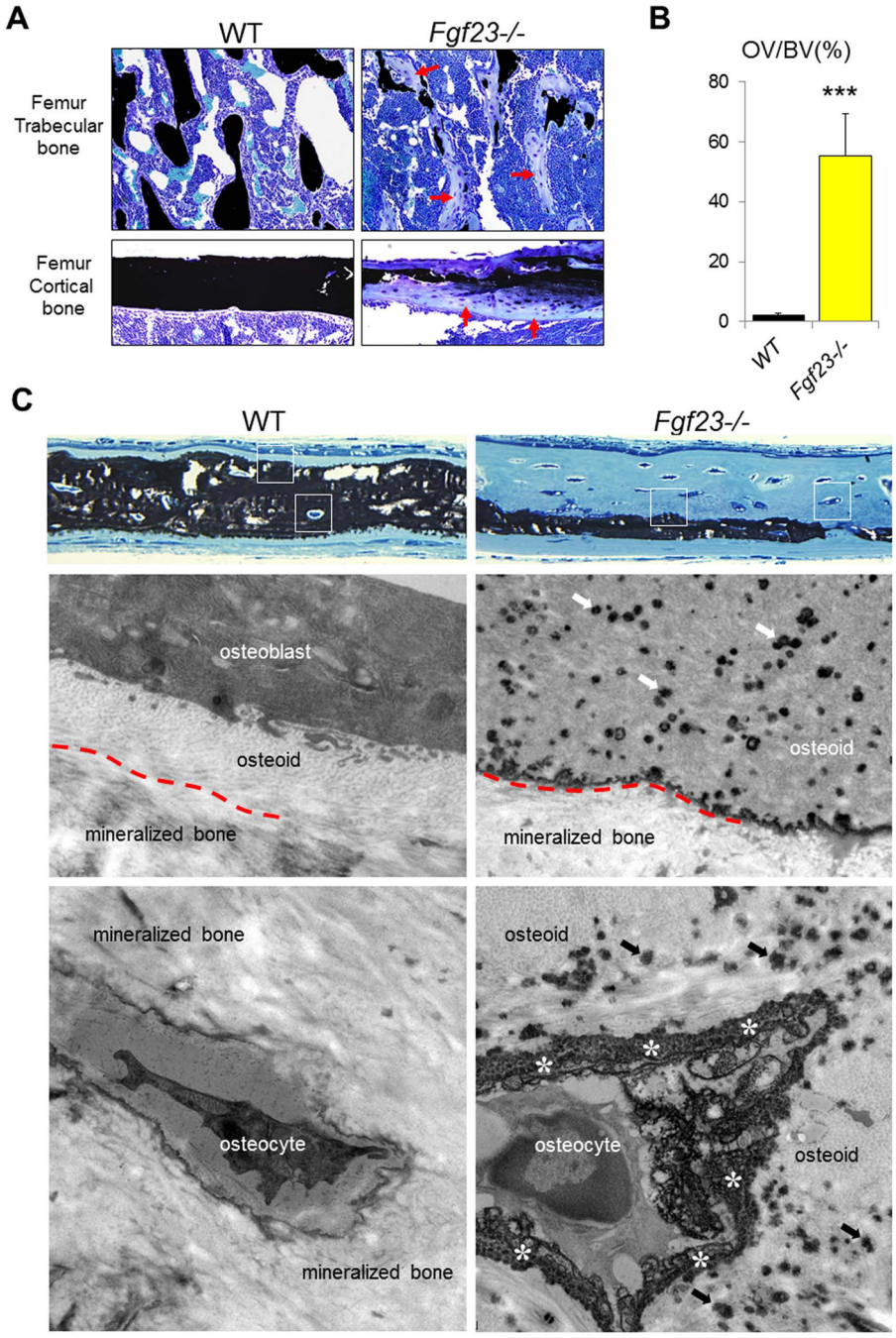

Figure 1. Defective skeletal mineralization of *Fgf23*$^{-/-}$ mice

(A) Representative images of undecalcified sections of femurs stained with von Kossa reagent for mineral (black) and counter stained with toluidine blue. Accumulation of osteoid (indicated by red arrows) is prominent in trabecular and cortical bone of *Fgf23*$^{-/-}$ mice. (B) Quantification of the osteoid volume (OV/BV) in trabecular bone. (C) Light micrographs (upper two panels) and electron micrographs (lower four panels whose approximate locations are framed by white boxes) of 3-wk-old undecalcified calvariae. By light microscopy, the normal bone in *WT* mice shows full-thickness mineralization with thin unmineralized osteoid seams. Transmission electron microscopy of *WT* bone shows

osteoblasts closely opposed to the osteoid surface, osteocytes embedded within mineralized bone, and the presence of an indistinct mineralization front (red dashed line) separating the osteoid from the mineralized bone. In *Fgf23*$^{-/-}$ calvarial bone, greatly widened osteoid seems are present, with a speckling in the innermost regions of the osteoid that were revealed by electron microscopy to be abundant aborted mineralization foci (arrows) in a generally unmineralized osteoid. In deeper regions that were in fact well mineralized, the mineralization front (red dashed line) was sharply delineated as an electron-dense boundary indicating a termination of mineralization at this site. Immediately surrounding osteocytes in this widened osteoid was a peripheral accumulation at the lacunar wall of finely granular mineral deposits (asterisks). Data are presented as Mean ± SD. ***: $p<0.001$ *vs WT*.

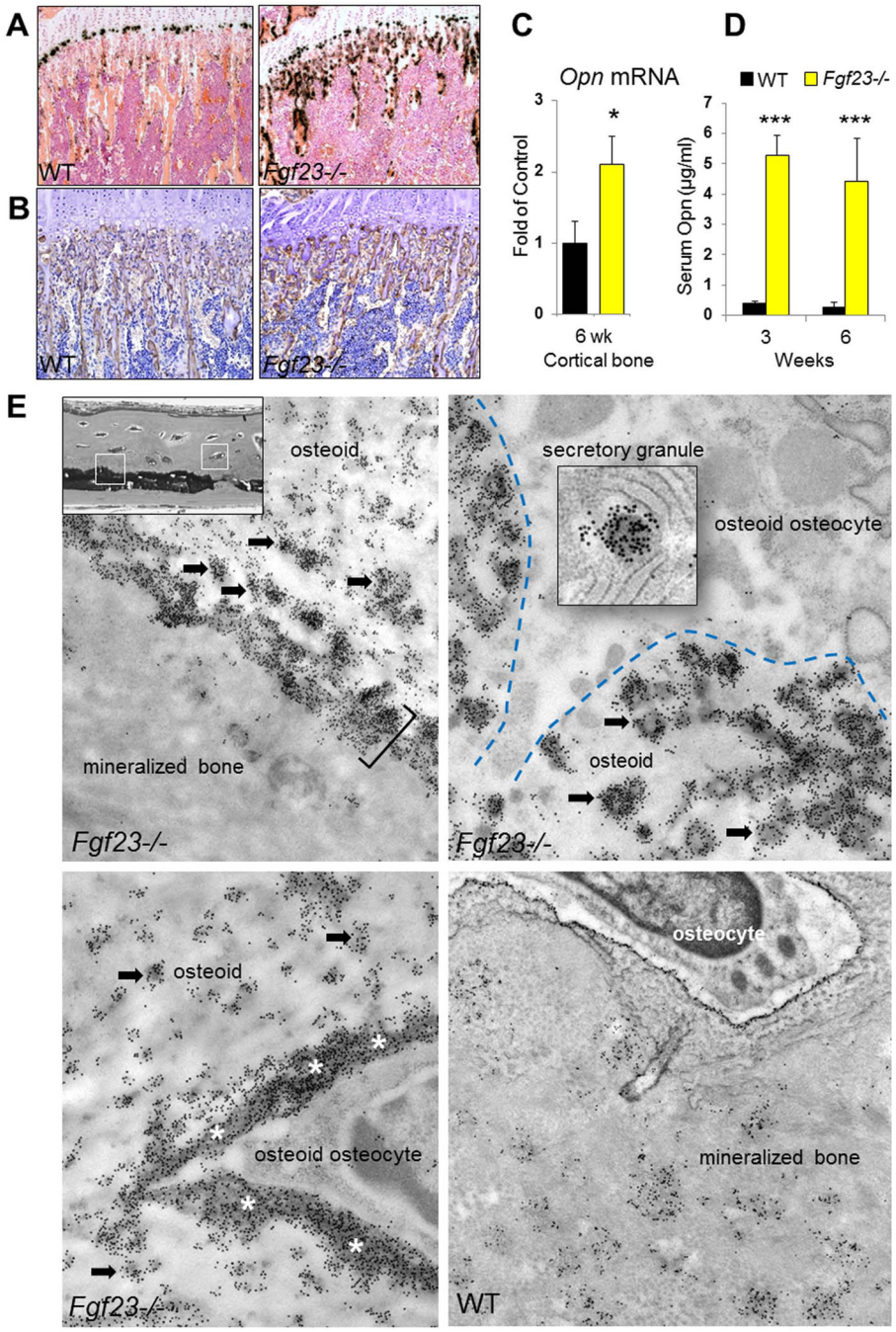

Figure 2. Increased OPN levels in *Fgf23*$^{-/-}$ mice

(A) In situ hybridization and (B) immunohistochemistry staining performed on femur sections of 6-week-old animals. Both showed increased OPN signals in *Fgf23*$^{-/-}$ bone. (C) mRNA expression of *Opn* in the cortical bones (femur) quantified by qRT-PCR analysis. (D) Serum OPN measurements. (E) Transmission electron micrographs after immunogold labeling for OPN in undecalcified calvarial bone at the locations framed by the white boxes. Compared to the moderate extent of immunolabeling of *WT* bone seen as patches of gold particles dispersed throughout the matrix and surrounding osteocyte lacunae. The bone of *Fgf23*$^{-/-}$ is intensely labeled at several locations. Abundant gold-particle labeling is

observed over the aborted mineralization foci (arrows) in the osteoid, at the sharply demarcated mineralization front (bracket), and immediately lining the lacunar wall (asterisks) surrounding osteocytes. Osteocytes found in these heavily OPN-labeled regions of osteoid bone matrix show prominent secretory granules intensely labeled for OPN indicating the local secretion of this protein by bone cells. The blue dashed line indicates the cell-matrix interface. Data are presented as Mean ± SD. *: $p<0.05$, ***: $p<0.001$ *vs WT*.

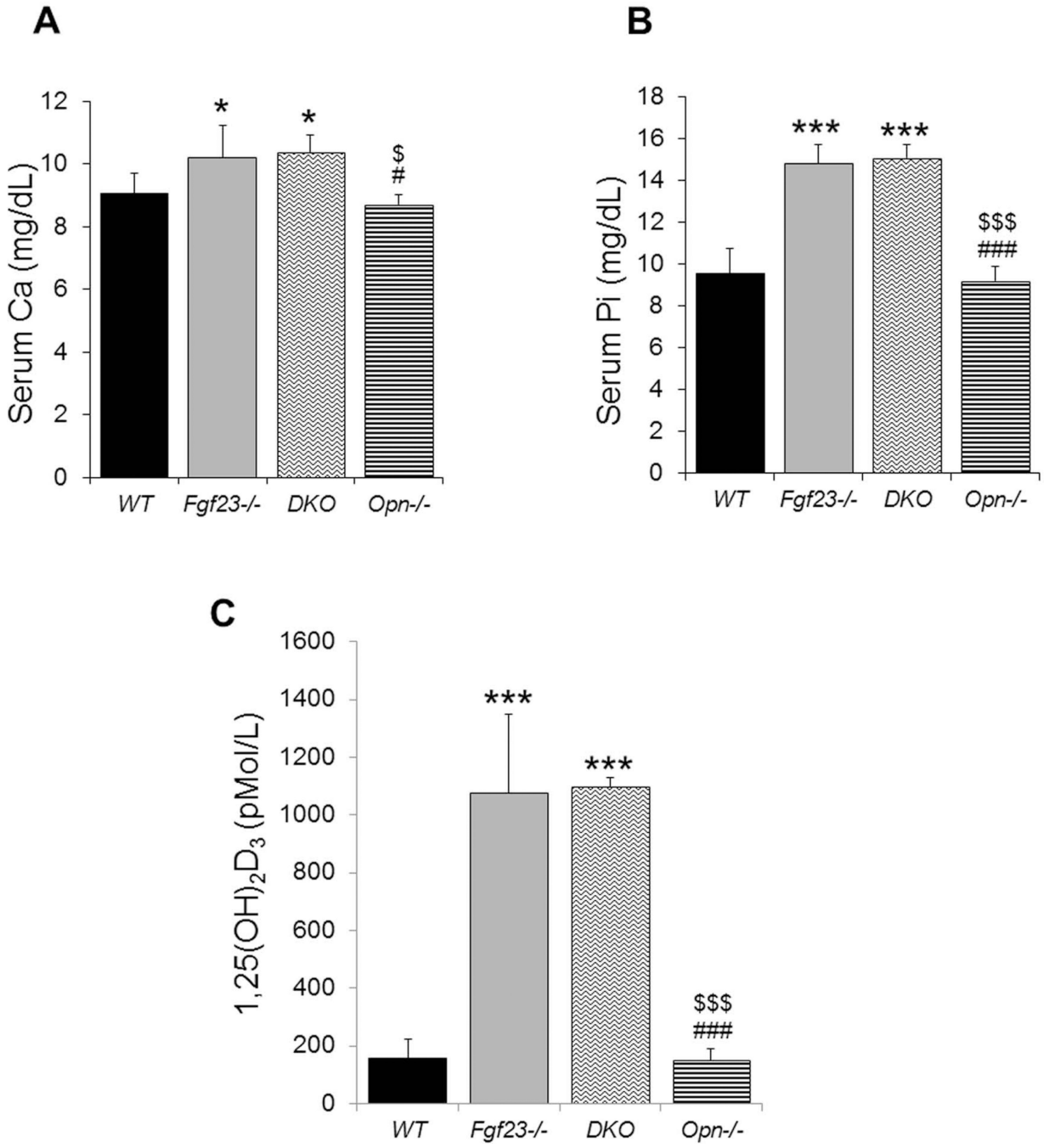

Figure 3. Serum biochemical measurements

Fgf23$^{-/-}$ and *DKO* mice show similarly increased levels of serum calcium (A), phosphate (B), and 1,25$(OH)_2$D (C). Data are presented as Mean ± SD. *: $p<0.05$, ***: $p<0.001$*vs WT*; #: $p<0.05$, ###: $p<0.001$*vs Fgf23*$^{-/-}$; and $: $p<0.05$, $$$: $p<0.001$ *vs DKO*.

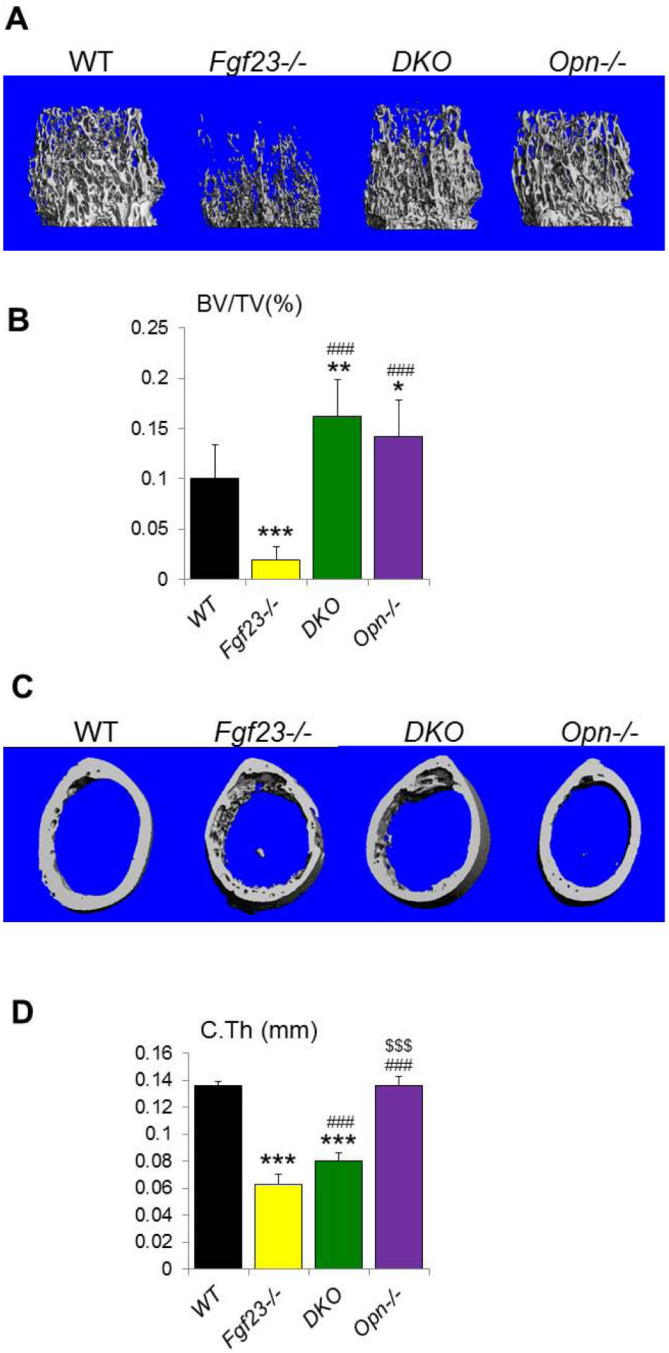

Figure 4. μCT analyses

(A) Representative images of 3D reconstruction of distal femoral metaphyses. (B) Trabecular bone volume fraction (BV/TV) is significantly increased in *DKO*. (C) Representative images of 3D reconstructions of midshaft cortical bone. (D) The cortical thickness (C.Th) of *DKO* bone is improved compared to that of $Fgf23^{-/-}$ bone. Data are presented as Mean ± SD. *: $p<0.05$, **: $p<0.01$, ***: $p<0.001$*vs WT*; ###: $p<0.001$*vs* $Fgf23^{-/-}$; and $$$: $p<0.001$ *vs DKO*.

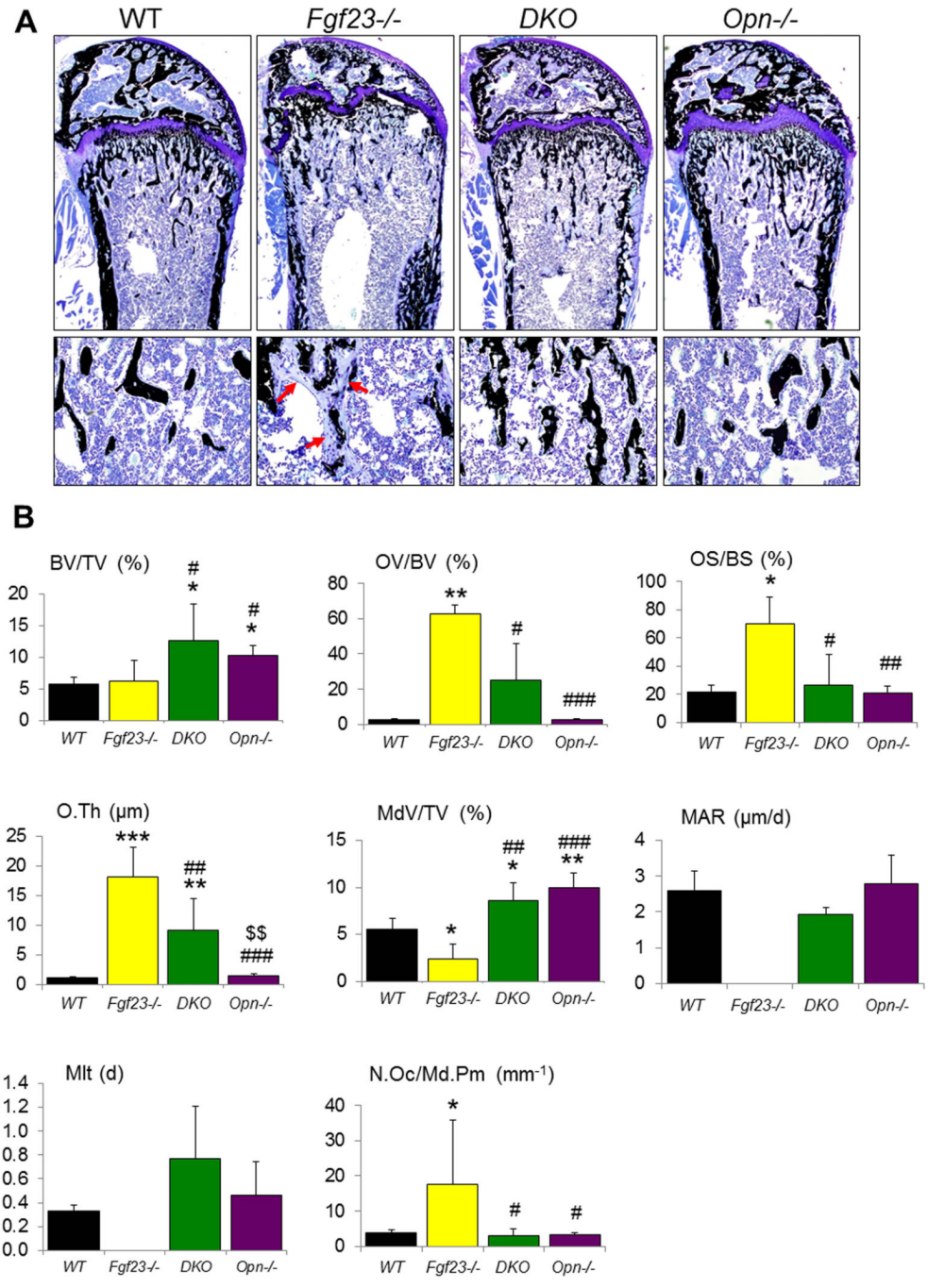

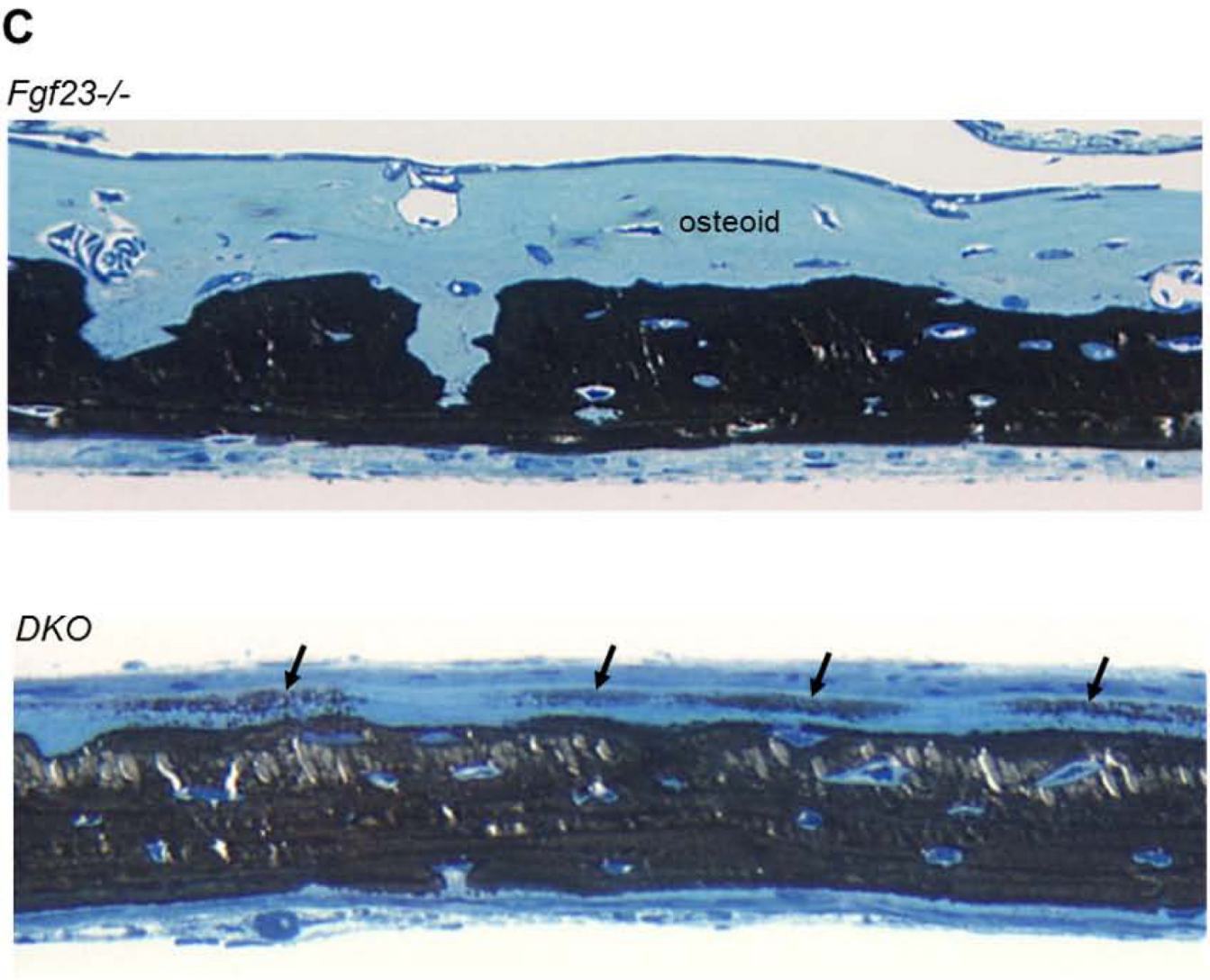

Figure 5. Histological and histomorphometric analyses

(A) Representative images of undecalcified sections of distal ends of femurs from 6wk-old littermates stained with von Kossa and McNeal stains. Red arrows indicate the large amount of unmineralized osteoid in *Fgf23*$^{-/-}$ bone. (B) Histomorphometric analysis confirmed that the mineralization defect of *Fgf23*$^{-/-}$ bone was partially rescued in *DKO* mice. BV/TV: bone volume; OV/TV: osteoid volume; OS/BS: osteoid surface; O.Th: osteoid thickness; Md.V/TV: mineralized trabecular bone volume; MAR: mineral apposition rate; and Mlt: mineralization lag time; N.Oc/Md.Pm: osteoclast number/mineralized bone perimeter. (C) Light micrographs of 3-wk-old undecalcified calvarial bone after von Kossa staining for mineral. Whereas in the *Fgf23*$^{-/-}$ mice the osteoidosis is severe, in the *DKO* calvariae there is an obvious decrease of osteoid thickness and with breakthrough isolated “islands” of mineralization (arrows) extending throughout the osteoid. Data are presented as Mean ± SD. *: $p<0.05$, **: $p<0.01$, ***: $p<0.001$ *vs WT*; and #: $p<0.05$, ##: $p<0.01$, ###: $p<0.001$ *vs Fgf23*$^{-/-}$; $$: $p<0.01$ *vs DKO*.

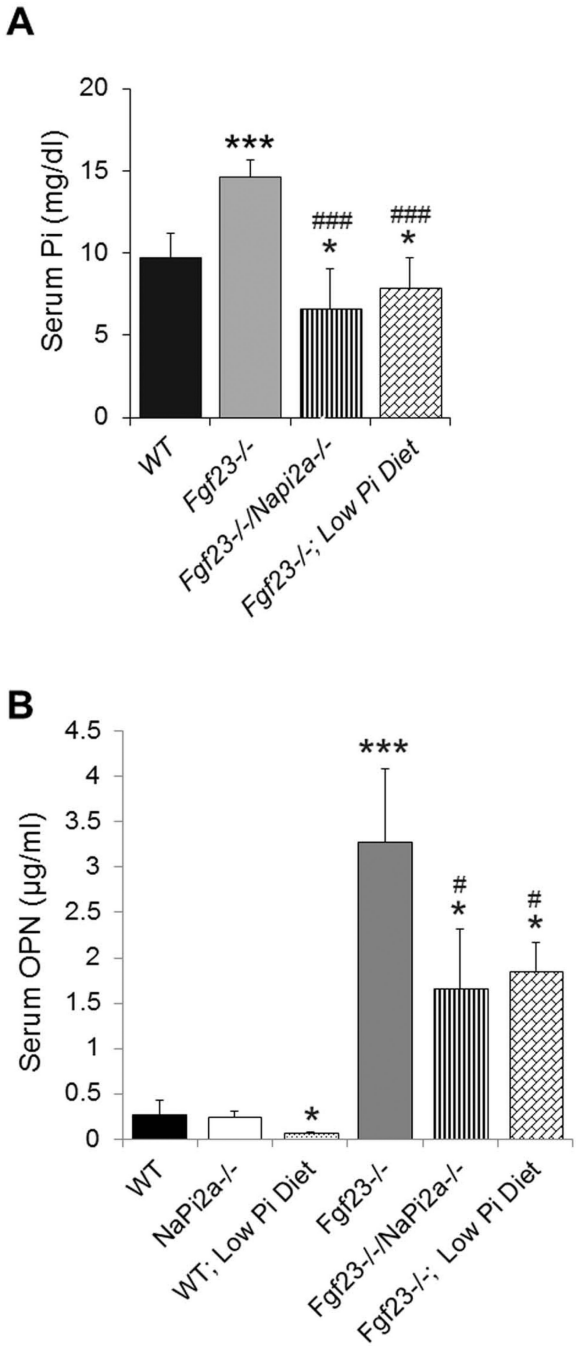

Figure 6. Decreased serum OPN levels upon lowering of serum phosphate

(A) Serum phosphate levels of mice with corresponding genotypes are shown. The hyperphosphatemia of *Fgf23*$^{-/-}$ mice was reversed to hypophosphatemia by deleting *NaPi2a* (*Fgf23*$^{-/-}$/*Napi2a*$^{-/-}$) or by feeding a low-phosphate diet (*Fgf23*$^{-/-}$; *Low Pi Diet*). (B) The high serum OPN levels of *Fgf23*$^{-/-}$ significantly decreased upon lowering serum phosphate levels in *Fgf23*$^{-/-}$/*NaPi2a*$^{-/-}$ *and Fgf23*$^{-/-}$; *Low Pi Diet* mice, but remained markedly higher than in wild-type (WT), *NaPi2a*$^{-/-}$ or *wild-type* mice fed a low-Pi diet *(WT; Low Pi Diet)*. Data are presented as Mean ± SD. *: $p<0.05$, ***: $p<0.001$ *vs WT*; #: $p<0.05$, ###: $p<0.001$ *vs Fgf23*$^{-/-}$.